Defect Depth Retrieval from Pulsed Phase Thermographic Data on Plexiglas and Aluminum Samples

C. Ibarra-Castanedo and X. Maldague[*]

Computer Vision and Systems Laboratory, Dept. of Electrical and Computer Engineering
Université Laval, Quebec City, Canada, G1K 7P4.

ABSTRACT

In the last few years, several quantitative inversion methods have been proposed to analyze pulsed phase thermographic data: statistical methods [1], Neural Networks [2] and wavelets [3], with a wide range of reported accuracies. In the present paper a new approach is proposed based on absolute phase contrast computations defined in a similar way as for absolute temperature contrast [4]. Phase contrast data is then used to estimate the *blind frequency*, *i.e.* the frequency at which the defect becomes visible for the 'first' time [5]. It was found an excellent agreement between defect depth z, and the corresponding blind frequencies f_b. Experimental tests on Plexiglas® and aluminum specimens demonstrate the potential of the technique on retrieving the depth of flat-bottomed holes. We also discuss temporal aliasing and its relationship with the phase delay images. As will be stressed, the unavoidable differences between the Continuous and the Discrete Fourier Transform of a time-dependent temperature decay signal can be effectively minimized not only by selecting a sampling frequency rate according to Shannon's Sampling Theorem (as is well-known [6]), but also by choosing an appropriate truncation window size [7].

Keywords: Pulsed Phase Thermography, Phase Contrast, Blind Frequency, Time Aliasing, Truncation.

INTRODUCTION

Pulse Thermography (PT) has been widely used on Nondestructive testing and Evaluation (NDT&E), not only for defect detection purposes but also to estimate the location, shape and size of defects. However, non-uniform heating, surface material emissivity and specimen geometry problems are usually present complicating the quantification of subsurface features. Lock-In Thermography (LT) and Pulsed Phase Thermography (PPT) are less affected by these problems thanks to the availability of phase delay images. There exist however some important differences between these two techniques. In LT, thermal waves at specific modular frequencies are used to heat the samples on a stationary regime and requires carrying out a different experience for every depth that is been investigated. On the other hand, PPT uses a transitory heat pulse (in a similar way as for PT) and phase images are obtained by post-processing of the signal. As a result, a single experience allows to evaluate different depths by unscrambling the frequencies using a transformation algorithm. The Fourier Transform was originally proposed [8], nevertheless, other transformations can be used, *e.g.* the Wavelet Transform [3], or the Hartley Transform [9]. There have been some attempts to evaluate the potential of PPT for quantitative applications using for instance statistical methods [1], Neural Networks [2], and the Wavelet Transform [3] for depth retrieval. However, the calibration steps and lengthy computation subroutines precludes their use on most NDT&E applications. In this paper, a new approach is proposed based on the determination of the *blind frequency, f_b* (*i.e.* the phase frequency at which the defect becomes visible for the first time), which is directly linked to the depth of the defect. Moreover, as will be stressed, the relationship between the Continuous Fourier Transform (CFT) and the Discrete Fourier Transform (DFT) of a time-dependent temperature signal is dictated predominantly by the sampling frequency, and by the size of the truncation window [7]. Furthermore, the sampling frequency in one domain is linked to the truncation window size on the other domain. As a consequence, large truncation windows in the time domain produce finely spaced data on the frequency spectra. Therefore, to better approximate the CFT, the length of the truncation window should be as long as possible, and the sampling frequency should be at least twice the Nyquist frequency as stipulated by Shannon's Sampling Theorem. The fundamental concepts concerning sampling theory are discussed in detail on reference [10]. In the following section we present a review on PPT theory.

---

[*] Corresponding author. Tel.: + 1-418-656-2962; fax: + 1-418-656-3594, Email address: maldagx@gel.ulaval.ca

1. PULSED PHASE THEMOGRAPHY (PPT)

1.1. Data acquisition

The procedure to perform a PPT experience is basically the same as for PT, a typical configuration is depicted on Figure 3a. The sample's surface is heated with a thermal pulse (*e.g.* using photographic flashes), after what, a thermal mapping of the surface or *thermogram* is recorded using an infrared camera and a PC. This procedure is repeated every Δt seconds until an *N*-element thermogram sequence is obtained. As shown in Figure 1a, a three-dimensional matrix is formed with *x* and *y* coordinates being the horizontal and vertical pixel positions respectively, and the *z*-coordinate corresponding to the time evolution.
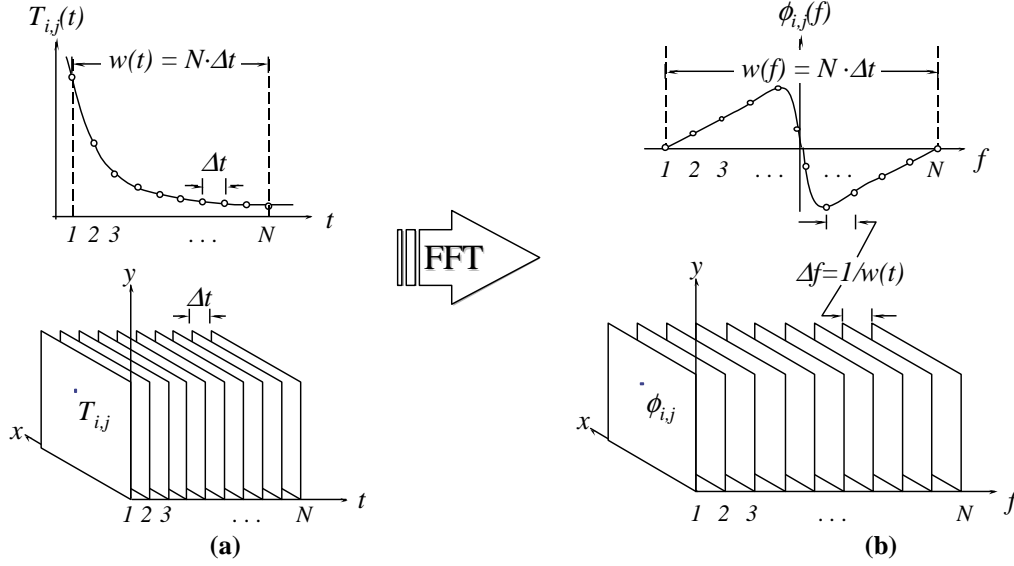

Figure 1. (a) Thermogram sequence and temperature profile for a pixel, and (b) phasegram sequence after application of the FFT.

1.2. Data processing using the Fourier Transform

Once the temperature data has been recorded, the entire sequence can be processed, at the pixel level, using the one-dimensional DFT [8]:

$$F_n = \sum_{k=0}^{N} T(k)e^{2\pi jkn/N} = \mathrm{Re}_n + \mathrm{Im}_n \tag{1}$$

where *j* is an imaginary number, *n* designates the frequency increment, and *Re* and *Im* are the real and the imaginary parts of the transform, respectively. For NDT&E applications, equation (1) is not practical due to lengthy computations. The Fast Fourier Transform (FFT) algorithm [11] greatly reduces the computation timing and is therefore privileged in this case. With the real and imaginary parts of the transform, phase delay ϕ, for a pixel becomes available as follows:

$$\phi = \tan^{-1}\left(\mathrm{Im}_n / \mathrm{Re}_n\right) \tag{2}$$

The procedure is repeated for all the pixels on the sequence to form phase maps or *phasegrams*, as shown on Figure 1b.

1.3. Phase properties

Contrary to thermograms, phasegrams have shown to be insensitive to reflections from the environment [5], to surface emissivity variations [12], to non-uniform heating [2] and to surface geometry [13]. Phase is therefore of particular interest for quantitative NDT&E applications. Depth probing reported values using phase data range from 1.8μ [12] to more than 2μ [14], where μ is the thermal diffusion length equation given by [4]: $\mu=(\alpha/\pi f)^{1/2}$. Inversion procedures using the phase are possible if we consider that the spectra representation of a function contains exactly the same information as the original signal [15]. For this to be true, discrete data must approach the continuous signal with good enough accuracy [10]. A new approach for depth retrieval using phase delay data is introduced in section 2.

2. DEPTH RETRIEVAL FROM PHASE CONTRAST DATA

2.1. Phase Contrast
The absolute phase contrast $\Delta\phi$, can be defined on a similar way as for absolute temperature contrast [5], [16]:

$$\Delta\phi = \phi_d - \phi_s \tag{3}$$

where ϕ_d is the phase of a defective pixel, and ϕ_s is the mean phase value of a defined sound area. Phase contrast depends on the thermal properties of the material, the subsurface structure of the sample, the modulation frequency and the subsurface heat transfer coefficient [5].

2.2. Blind frequency, f_b
As is well known [4], deeper defects are detected at low frequencies while only shallow defects are visible at high frequencies. Therefore, a thick defect (flat-bottomed hole) can be seen from the minimum available frequency (see Figure 2) to a specific higher frequency for which the $\Delta\phi$ is not large enough for the defect to be detected.
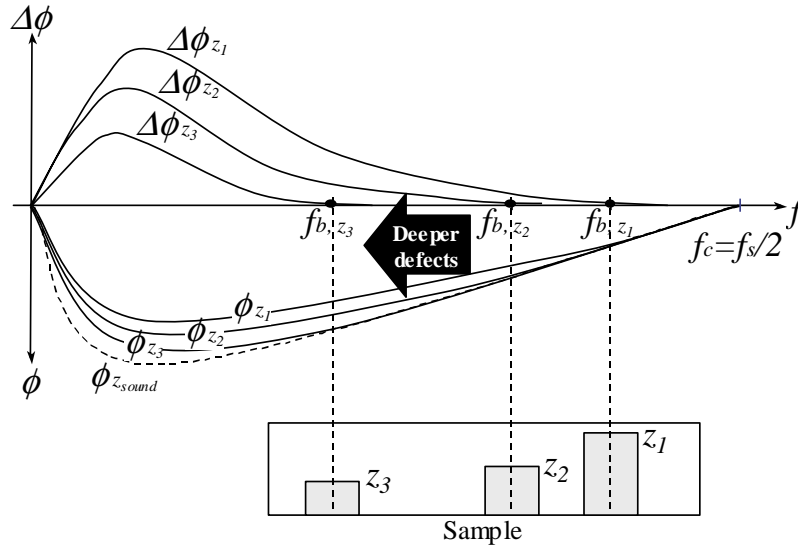

Figure 2. Blind frequency relationship with defect depth.

Theoretically, the limiting phase contrast should be $\Delta\phi$=0. In practice however, phase data is contaminated with noise and a threshold contrast value must be set in some cases. For instance, Bai and Wong [5] reported that a phase contrast value of $\Delta\phi$>5° (0.87 rad), was enough for an 11 mm defect at a 1.4 mm depth to be visible on CRFP composites plates. The corresponding frequency at which the defect becomes visible for the first time is called the *blind frequency* or f_b. From the diffusion length equation defined by Eq. (3), and the phase delay definition ($\phi=z/\mu$) [4], depth z, changes inversely with the square root of the depth of the defect [17]:

$$z \propto f_b^{-1/2} \tag{4}$$

Deeper defects disappear at a lower frequency with respect to shallower defects. This is schematized on Figure 2 for three flat-bottomed holes at different depths. The phase profiles ϕ, are shown on the bottom part of the y-axis. Phase contrast curves $\Delta\phi$, are calculated with equation (3) using the phase of a sound area (dotted curve), and they are shown on the top part of the y-axis. The shallowest defect is visible ($\Delta\phi$>0) at low and high frequencies while the deepest defect is only detected at low frequencies. With respect to LT, PPT has the advantage that several frequencies are available on a single heat pulse experience after performing the FFT. One single test is thus enough to estimate the blind frequency at several different depths. On the contrary, a distinct experience should be performed for every depth studied by LT. This procedure is not limited to flat-bottomed holes. For example, the defect thickness can be estimated by the difference between f_b and the corresponding frequency at which the defect reappears (with inverse sign) [12].

3. EXPERIMENTAL PROCEDURE

3.1. Experimental Setup

The experimental setup is depicted on Figure 3a. Acquisition was carried out using a FPA infrared camera (Santa Barbara Focalplane SBF125, 3 to 5 μm, with a 320x256 pixel array), working at a sampling frequency of 0.28 Hz for the Plexiglas® plate and at 45.1 Hz for the aluminum plate. Two high power photographic flashes (Balcar FX 60), giving 6.4 kJ for 15 ms each, were used as heating sources. Thermographic data was analyzed with a PC (Pentium 4, 2 GB RAM), and thermal data was processed using MatLab® language from The MathWorks, Inc.
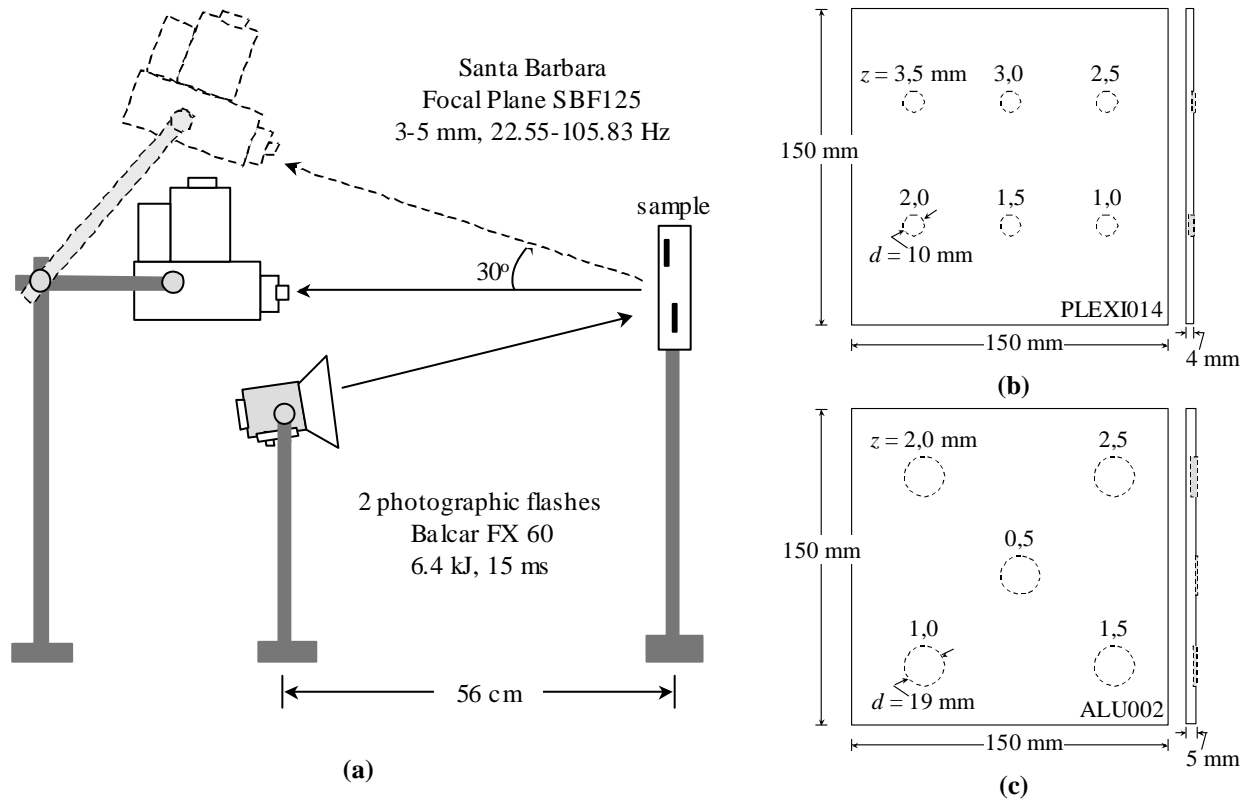

Figure 3. (a) Experimental setup, (b) Plexiglas® sample (PLEXI014) and (c) aluminum sample (ALU001).

3.2. Specimens

The samples dimensions for Plexiglas® and aluminum plates are shown on Figure 3b and c, respectively. The 4 mm thick Plexiglas® plate (PLEXI014) has 6 artificial defects (flat-bottomed holes) 10 mm in diameter at 3.5, 3, 2.5, 2, 1.5 and 1 mm depth. Flat-bottomed holes for the 5 mm thick aluminum plate are 19 mm in diameter and they are located at 0.5, 1, 1.5, 2 and 2.5 mm depth. To test the impact of surface orientation on phase, two different configurations were tested for the Plexiglas® plate: 0° and 30° angle between the normal to the sample surface and the IR camera, see Figure 3a.

4. RESULTS

4.1. Low conductivity materials: Plexiglas® plate, 0° orientation

Phase and phase contrast profiles for the Plexiglas® plate shown on Figure 3b, are presented on Figure 4. Data on this figures, shows a strong relationship between defect depth and blind frequency. Phase profiles for the shallowest defects differ sharply from the sound area phase profiles. This is because sound area corresponds to Plexiglas® material exclusively, while for the shallowest defect, Plexiglas® is present from the surface to 1 mm depth and the rest (from 1 to 4 mm depth) is filled with air. Defects phase profiles are more and more like sound area profiles as we go deeper. The blind frequency, as well as the maximum phase contrast value, decreases with defect depth as seen on Figure 4b.

The frequency range of visibility for the shallowest defect is much wider than for the deepest defect. Figure 5 presents the phase images corresponding to the blind frequencies of the 6 defects of the Plexiglas® plate. All defects are visible on Figure 5a, which is the phasegram at the blind frequency for the deepest defect. Defects vanish one by one as phasegrams for shallower defects at the corresponding blind frequencies are shown until only the shallowest defect (1 mm depth) can be detected on Figure 5f. Also noted are the increasing noise levels for higher blind frequencies.
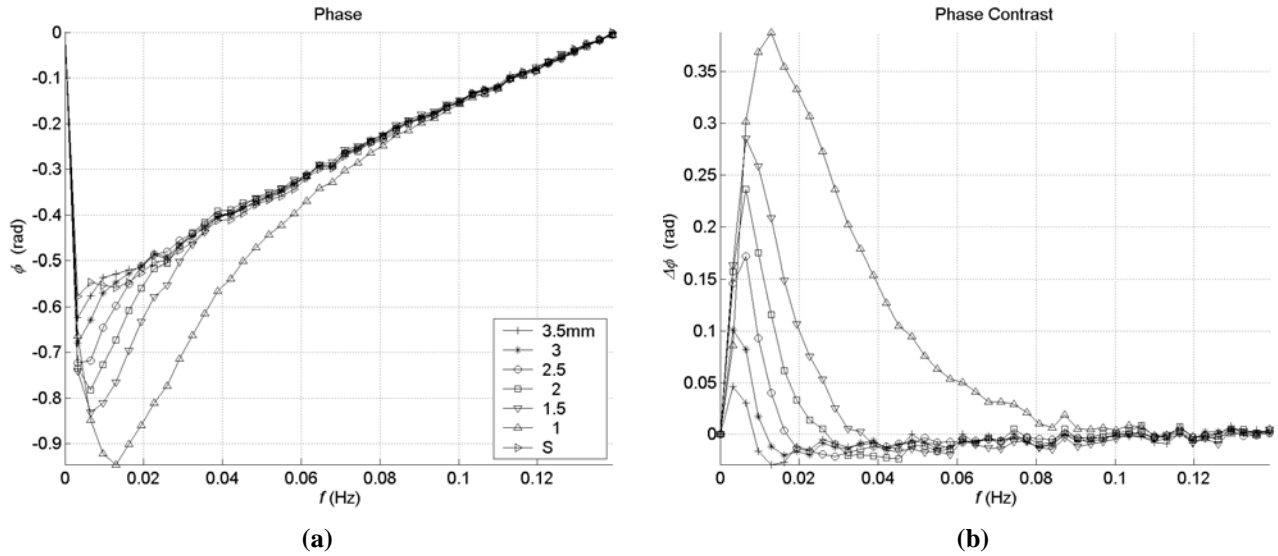

(a)   **(b)**

Figure 4. PLEXI0014, f_s=0.28 Hz, 0° orientation: (a) Phase and (b) phase contrast profiles.

(a)   **(b)**   **(c)**

(d)   **(e)**   **(f)**

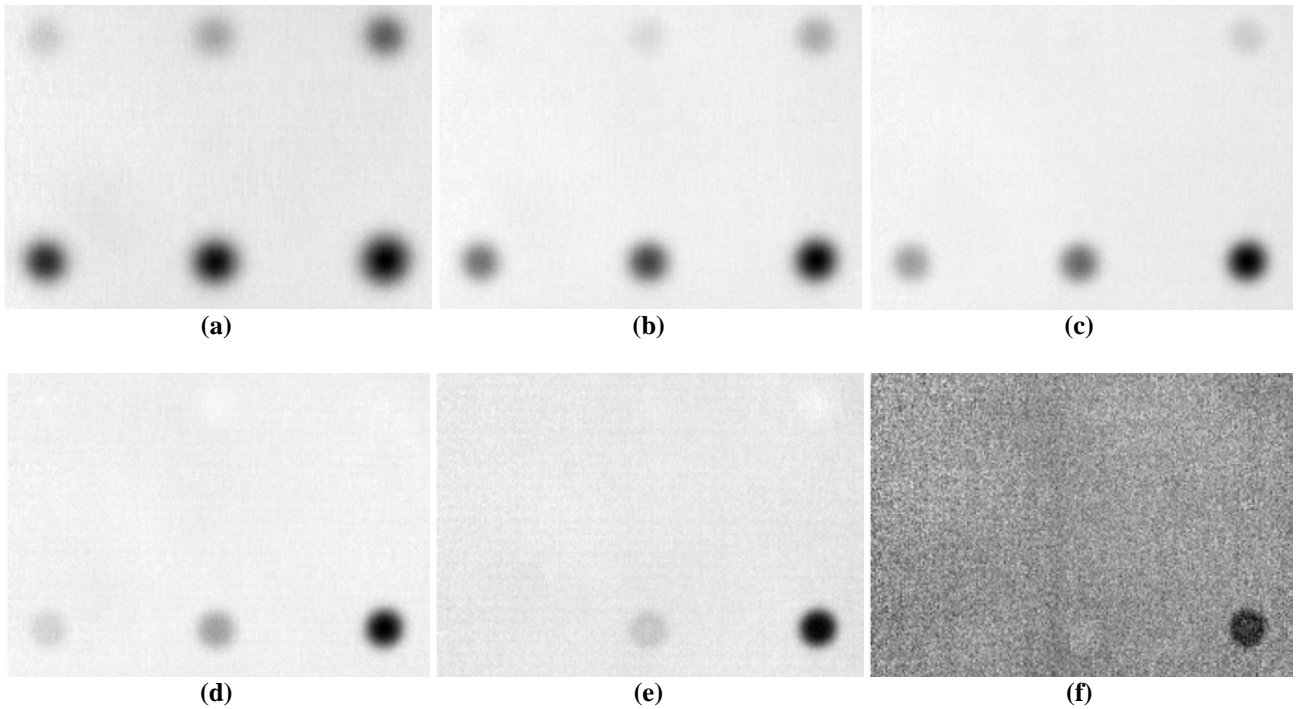Figure 5. PLEXI0014, f_s=0.28 Hz, 0° orientation: Phasegrams for the blind frequencies corresponding to the 6 different depths of the defects: (a) f_b (3.5 mm) = 0.0065 Hz, (b) f_b (3 mm) = 0. 0097 Hz, (c) f_b (2.5 mm) = 0.0162 Hz, (d) f_b (2 mm) = 0.0259 Hz, (e) f_b (1.5 mm) = 0.0356 Hz and (f) f_b (1 mm) = 0.1067 Hz.

The linear fitting on Figure 6b was obtained with the defect depths shown on Figure 6a, and the corresponding blind frequencies (Figure 5). A very high correlation coefficient was obtained (R=0.99492).
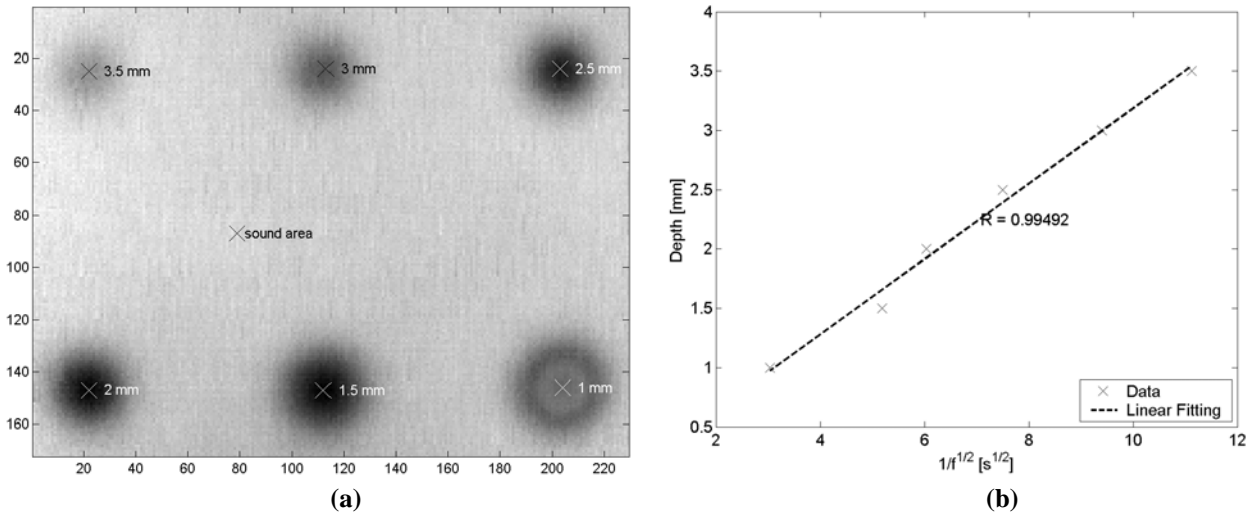

| (a) | (b) |

Figure 6. PLEXI0014, f_s=0.28 Hz, 0° orientation: (a) Defect's depths and location, and (b) depth vs frequency linear fitting.

4.2. Low conductivity materials: Plexiglas® plate, 30° orientation

The same procedure was follow for an oriented Plexiglas® plate. Phase and phase contrast profiles are shown on Figure 7, and a phasegram showing the defect depths and the fitting results are presented on Figure 8. Defects on Figure 8a appear distorted (ellipses instead of circles) because of the plate orientation with respect to the IR camera. Linear correlation still holds for this case with a very high correlation coefficient (R=0.99472) as seen on Figure 8b.
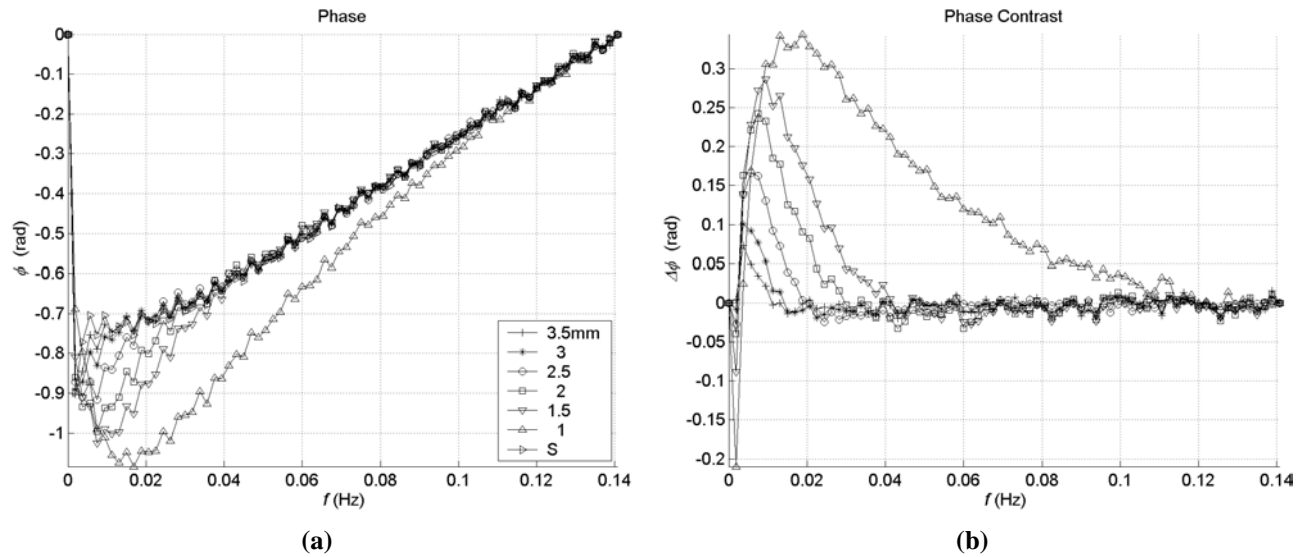

| (a) | (b) |

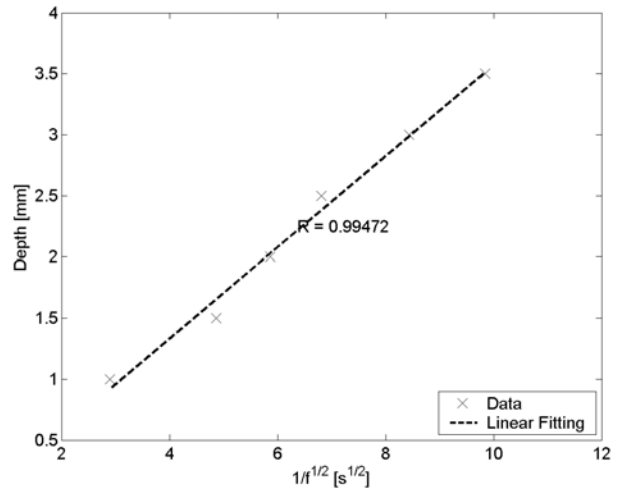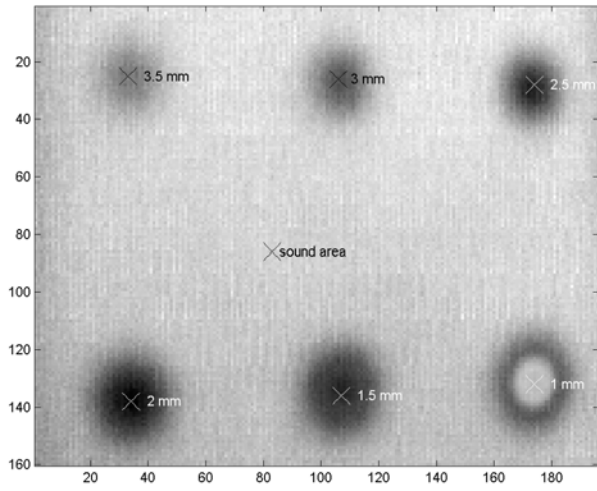Figure 7. PLEXI0014, f_s=0.28 Hz, 30° orientation: (a) Phase, and (b) phase contrast profiles.

Figure 8. PLEXI0014, f_s=0.28 Hz, 30° orientation: (a) defect's depths and location, and (b) depth vs frequency linear fitting.

4.3. High conductivity material: aluminum plate

An aluminum plate was also tested. Figure 9 shows the phase and phase contrast profiles. A much higher frequency rate (45.1 Hz) than the sampling rate used for Plexiglas®, was required on this case to be able to record enough information on this high conductivity material. A 0.1 rad threshold was set as the limiting phase contrast. The 2.5 mm defect did not produce enough contrast and the corresponding data was discarded on the linear correlation shown on Figure 10b. Because of the time-frequency duality [10], better phase contrast values can be obtained using wider truncation windows (finer sampling on the frequency spectra).
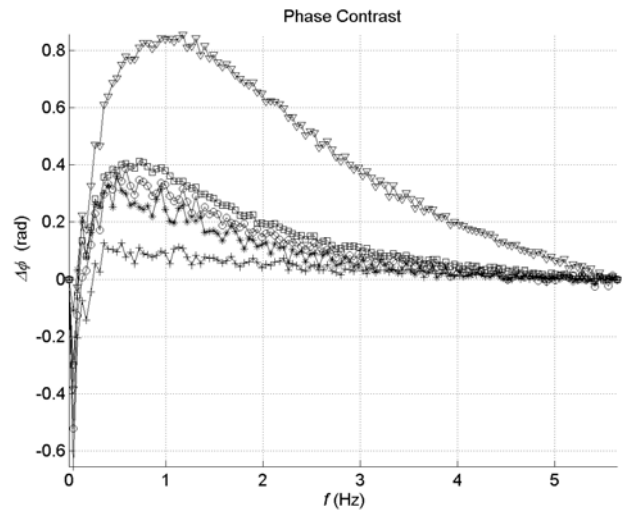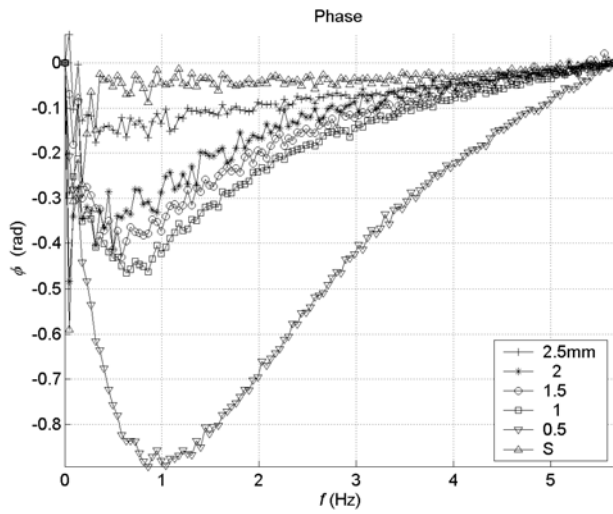

Figure 9. ALU002, f_s=45.1 Hz. (a) Phase, and (b) phase contrast profiles.
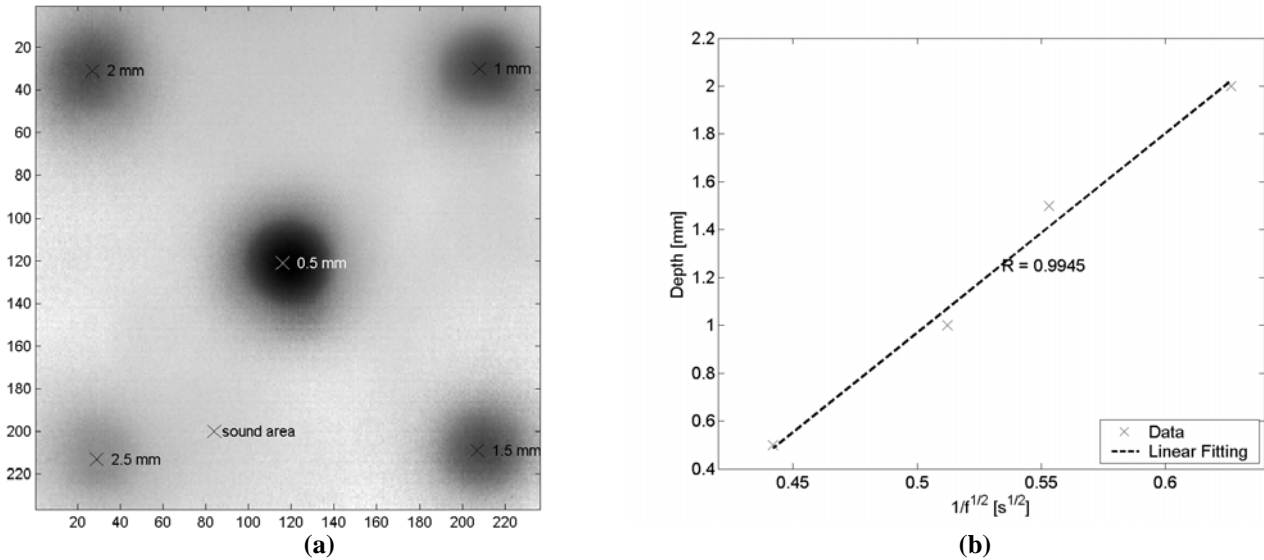
Figure 10. ALU002, f_s=45.1 Hz, $\Delta\phi$=0.1 rad. (a) Defect's depths and location, (b) depth vs frequency linear fitting.

CONCLUSIONS

In this paper, the PPT principle is reviewed followed by an introduction of a new depth retrieval approach using phase delay data. Experimental results for low and high conductivity materials (Plexiglas® and aluminum) are presented as well. It was found in both cases, that depth is strongly related to the blind frequency (*i.e.* the frequency at which a defect is visible for the first time). Data was best fitted using linear fitting with a very high correlation coefficient both for low and high conductivity materials. Moreover, a high correlation coefficient was still obtained for an oriented Plexiglas® plate, confirming that phase is less affected than temperature by surface geometry variations. For instance, a 30° orientation with respect to the IR camera had virtually no effect on phase.

Low conductivity materials required lower sampling frequency rates as expected (0.28 Hz for Plexiglas® and 45.1 Hz for aluminum). The necessity for high sampling rates on high conductivity materials is compensated only in part by the narrower truncation window size requirement (533 s for Plexiglas® and 11 s for aluminum). Nevertheless, depth range for Plexiglas® was still greater than for aluminum (1 to 3.5 mm for Plexiglas® and 0.5 to 2 mm for aluminum). Sampling rate and truncation window size are therefore the two most important parameters to take into account to optimize depth retrieval procedures. For instance, the 2.5 mm defect on the aluminum plate didn't produce enough contrast to be used on the quantitative analysis. A wider truncation window would produce better results. The sampling rate and truncation window size values must be selected making a compromise between spectral resolution and the available computer power.

ACKNOWLEDGES

REFERENCES

1. VALLERAND S. and MALDAGUE X. "Defect Characterization in Pulsed Thermography: A Statistical Method Compared with Kohonen and Perceptron Neural Networks", *NDT&E International*, **33**: 307-315, 2000.
2. MALDAGUE X., LARGOUËT Y. and COUTURIER, J-P. "A Study of Defect Depth Using Neural Networks in Pulsed Phase Thermography: Modelling, Noise, Experiments", *Rev. Gén. Therm.*, **37**: 704-717, 1998.
3. GALMICHE F., MALDAGUE X. "Depth defect retrieval using the wavelet pulsed phased thermography," QIRT 2000 (Quantitative Infrared Thermography), Eurotherm Seminar 64, D. Balageas, G. Busse, C. Carlomagno (eds.), Reims, France, pp. 194-199, 2000.
4. MALDAGUE X. P. "Theory and practice of infrared technology for nondestructive testing", John Wiley & Sons, N.Y., 2001.
5. BAI W. and WONG B. S. "Evaluation of Defects in Composite Plates under Convective Environments using Lock-In Thermography", *Meas.Sci. Technol.,* **12**: 142-150, 2001.
6. GALMICHE F., LECLERC M. and MALDAGUE X. "Time Aliasing Problem in Pulsed Phased Thermography", in Rozlosnik A.E. and Dinwiddie R. D. (eds.), *Thermosense XXIII, SPIE Proc.,* **4360**: 550-553, 2001.
7. CASTLEMAN K. R. "Digital Image Processing", Prentice-Hall, Inc., Upper Saddle River, NJ, 1996.
8. MALDAGUE X. P. and MARINETTI S. "Pulse Phase Infrared Thermography", *J. Appl. Phys.*, **79**(5): 2694-2698, 1996.
9. PILLA M., KLEIN M., MALDAGUE X. and SALERNO A., "New Absolute Contrast for Pulsed Thermography," in D. Balageas, G. Busse, C. Carlomagno (eds.), *Proc. QIRT 2002 (Quantitative Infrared Thermography)*, Dubrovnik, Croatia, 2002.
10. IBARRA-CASTANEDO C. and MALDAGUE X. "Pulsed Phase Thermography Reviewed" *accepted for publication in Journal of Qirt 7*, 2004 (in press).
11. COOLEY J. W. and TUKEY J. W. "An Algorithm for the Machine Calculation of Complex Fourier Series", *Mathematics of Computation*, **19**(90): 297-301, 1965.
12. GIORLEO G. and MEOLA C. "Comparison between Pulsed and Modulated Thermography in Glass-Epoxy Laminates", *NDT&E International*, **35**: 287-292, 2002.
13. MALDAGUE X. and COUTURIER, J-P. "Review of Pulse Phase Infrared Thermography" in Abbozzo L.R., Carlomagno G.M., Corsi C. (eds.), *IV International Workshop on Advanced Infrared Technology and Applications Atti della Fondazione G. Ronchi*, Firenze (Italy), September 15-16 1997.
14. BUSSE G. and ROSENCWAIG A. "Subsurface Imaging with Phase Sensitive Modulated Thermography", *Appl. Phys. Lett.*, **36**: 815-816, 1980.
15. BRIGHMAN E. O. "The Fast Fourier Transform", Prentice-Hall, Inc., Englewood Cliffs, NJ, 1974.
16. SAKAGAMI T., KUBO S., NAKAMURA S., KAWASHIMA Y. and KOMIYAMA T. "Application of Lock-In Data Processing for Thermographic NDT of Concrete Structures", in Maldague X. P. and Rozlosnik A. E. (eds.), *Thermosense XXIV,* **4710**: 552-557, 2002.
17. IBARRA-CASTANEDO C., GONZÁLEZ D., KLEIN M. PILLA M., VALLERAND S. and MALDAGUE X. "Infrared Image Processing and Data Analysis" *VII Workshop on Advances in Infrared Technology and Applications (7th AITA)*, Pisa (Italy) September 9-11, 2003.
18. BRACEWELL R. "The Fourier Transform and its Applications", McGraw-Hill, 1965.
19. BUSSE G., WU D. et KARPEN W. "Thermal Wave Imaging with Phase Sensitive Modulated Thermography", *J. Appl. Phys.*, **71**(8): 3962-3965, 1992.
20. FAVRO L. D. and HAN X. "Thermal Wave Materials Characterization and Thermal Wave Imaging", in Birnbaum G., Auld B. A. (eds.), *Sensing for Materials Characterization, Processing and Manufacuring*, ASNT TONES, **1**: 399-415, 1998.